Atmos. Chem. Phys. Discuss., 14, 7141–7186, 2014
www.atmos-chem-phys-discuss.net/14/7141/2014/
doi:10.5194/acpd-14-7141-2014

Atmospheric Chemistry and Physics Discussions

Impact of heterogeneous ice nucleation by natural dust and soot based on a probability density function of contact angle model with the Community Atmospheric Model version 5

Y. Wang[1,2,3], X. Liu[2], C. Hoose[4], and B. Wang[1]

[1]Institute of Atmospheric Physics, Chinese Academy of Sciences, Beijing 100029, China
[2]Department of Atmospheric Science, University of Wyoming, Laramie, WY 82071, USA
[3]University of Chinese Academy of Sciences, Beijing 100049, China
[4]Karlsruhe Institute of Technology, Institute for Meteorology and Climate Research, 76131 Karlsruhe, Germany

Received: 4 March 2014 – Accepted: 6 March 2014 – Published: 18 March 2014

Correspondence to: X. Liu (xliu6@uwyo.edu)

Published by Copernicus Publications on behalf of the European Geosciences Union.

Abstract

In order to investigate the impact of different treatments for the contact angle (α) in heterogeneous ice nucleating properties of natural dust and black carbon (BC) particles, we implement the classical-nucleation-theory-based parameterization of heterogeneous ice nucleation (Hoose et al., 2010) in the Community Atmospheric Model version 5 (CAM5), and then improve it by replacing the original single contact angle model with the probability density function of α (α-PDF) model to better represent the ice nucleation behavior of natural dust found in observations. We re-fit the classical nucleation theory (CNT) to constrain the uncertain parameters (i.e., onset α and activation energy in the single α model; mean contact angle and standard deviation in the α-PDF model) using recent observation datasets for Saharan natural dust and BC (soot). We investigate the impact of time-dependence of droplet freezing on mixed-phase clouds and climate in CAM5, and the roles of natural dust and soot by different nucleation mechanisms. Our results show that when comparing with observations, the potential ice nuclei (IN) calculated by the α-PDF model has a better agreement than that calculated by the single-α model at warm temperatures ($T > -20\,^{\circ}\mathrm{C}$). Ice crystals can form at lower altitudes (with warmer temperatures) simulated by the α-PDF model compared with the single-α model in CAM5. All of these can be attributed to different ice nucleation efficiencies among aerosol particles with some particles having smaller contact angles (higher efficiencies) in the α-PDF model. In the sensitivity tests with the α-PDF model, we find that the change of mean contact angle has larger impact on the active fraction than that of standard deviation, even though the change of standard deviation can lead to the transition of freezing behavior. Both the single α and the α-PDF model indicates that the immersion freezing of natural dust plays a more important role in the heterogeneous nucleation than that of soot in mixed-phase clouds.

ACPD
14, 7141–7186, 2014

1 Introduction

Ice microphysical processes in clouds are vital to cloud radiative properties and precipitation formation. They include the primary ice formation, vapor deposition on ice crystals, accretion of cloud droplets by ice crystals, ice aggregation and sedimentation, ice multiplication, sublimation, melting, and etc (Pruppacher and Klett, 1997; Morrison and Gettelman, 2008). Till now, ice formation mechanisms, especially by heterogeneous ice nucleation, have not been well understood. In mixed-phase clouds with temperatures between 0 and −38 °C, primary ice formation can be via the heterogeneous ice nucleation with the aid of a fraction of aerosol particles called ice nuclei (IN) (DeMott et al., 2010). Various particles can act as IN, which includes mineral dust, soot, volcanic ash, and primary biological particles (Hoose and Möhler, 2012; Murray et al., 2012).

Mineral dust has been recognized as the most important/atmospherically relevant IN either from the laboratory measurements or field sample studies (Hoose and Möhler, 2012; Murray et al., 2012). Natural mineral dust particles are often internally mixtures of different minerals, quartz and other components (Murray et al., 2012). In order to reduce the complexity encountered in natural mineral dusts, laboratory studies have often used commercially available pure minerals (Hoose and Möhler, 2012; Hoose et al., 2008). The most abundant minerals in the clay size fraction of mineral dust are kaolinite, illite and montmorillonite. On the other hand, a lot of laboratory experiments used commercially available Arizona Test Dust (ATD) as a surrogate for desert dusts (e.g., Knopf and Koop, 2006; Marcolli et al., 2007; Kulkarni et al., 2012). However, ATD can be more active than natural desert dust, either due to its enhanced roughness resulting from the milling or due to its different mineralogical composition (Möhler et al., 2006). Another reason for lower activity of natural dust particles is related to their aging processes in the atmosphere, which may reduce their ice nucleation ability (Sullivan et al., 2010).

Heterogeneous ice nucleation occurs via several different mechanisms (Vali, 1985), called nucleation modes (e.g., immersion, deposition, condensation, and contact freez-

ACPD
14, 7141–7186, 2014

ing). For immersion freezing, a supercooled cloud droplet containing an ice nucleus, by subsequent cooling, nucleates at a certain degree of supercooling. Prenni et al. (2007), through airborne measurements of IN number concentration and elemental composition from the US Department of Energy (DOE) Atmospheric Radiation Measurement (ARM) Mixed-Phase Arctic Clouds Experiment (M-PACE) in northern Alaska, found that immersion and/or condensation freezing (instruments can not separate them) may be the dominant freezing mechanism within these clouds. The term "deposition nucleation" describes that the vapor phase directly deposits on a dry ice nucleus and leads to the growth of ice. "Contact freezing" refers to the freezing of a supercooled droplet, which collides with a dry ice nucleus.

To represent the heterogeneous IN number and ice nucleation process, several heterogeneous freezing parameterizations have been developed, which can be divided into two groups: singular (or deterministic) hypothesis and stochastic hypothesis. The first, "singular (or deterministic) hypothesis" proposed by Langham and Mason (1958) assumes that the radius of the ice germ forming on the aerosol surface, at a given supercooling, is controlled by surface features, and thermal fluctuations have a negligible influence on ice germ radius. Thus, at the given supercooling, if an ice germ reaches the critical germ radius, the droplet will freeze immediately. Otherwise the droplet should still keep liquid state irrespective of the time (Niedermeier et al., 2010; Niemand et al., 2012; Phillips et al., 2008; DeMott et al., 2010). The second one, the "stochastic hypothesis" proposed by Bigg (1953), holds that heterogeneous ice nucleation is a function of time. During the time an immersed aerosol particle spends at constant environmental temperature, water molecules within supercooled water stay in the thermal fluctuation state of capturing and losing molecules to produce the clusters, which resemble the structure of ice. When some of these ice germs reach to a size (the critical radius), they become stable and initiate freezing. The presence of a particle surface immersed in a supercooled droplet is helpful for ice formatting by reducing the number of water molecules that are required to reach the stable cluster radius by letting the germ form on it as a spherical cap. The rate of heterogeneous nucleation per

ACPD
14, 7141–7186, 2014

aerosol particle and per time is referred to as the nucleation rate (J_{het}). This stochastic approach can be described by the classical nucleation theory (CNT) (Hoose et al., 2010; Niedermeier et al., 2011; Welti et al., 2012).

In CNT, J_{het} is proportional to the aerosol surface area and is the function of contact angle (α), which is the angle where ice germ/liquid or ice germ/vapor interface meets the aerosol surface, and can be understood as the surrogate of the nucleation ability of aerosol particles. The particle with the smaller contact angle (α) has higher ice nucleating efficiency. The contact angle is often derived from the fitting to the laboratory data, as done in Marcolli et al. (2007) for ATD, in Lüönd et al. (2010) for kaolinite, and in Wheeler and Bertram (2012) for kaolinite and illite. As noted in these studies, assuming that each particle has the same fixed contact angle often does not fit to the observation data well, especially when the observed ice nucleating fraction has weak time dependence. These authors suggested to use a probability density function of contact angles (α-PDF) instead of single values to better fit to the observed frozen fraction as a function of temperature (for immersion/condensation nucleation) or supersaturation (for deposition nucleation). In this α-PDF model, contact angles are distributed to every particle, which means that each particle has one value of the contact angle and that the particles with low contact angles are rapidly depleted when the temperature is held constant, thus leading to a slow-down of the freezing of the sample. The α-PDF model can be interpreted as an "intermediate" approach based on CNT between the two extremes of stochastic and singular hypotheses (Niedermeier et al., 2010).

Several heterogeneous ice nucleation parameterizations which are based on laboratory studies or in-situ measurements have been implemented in global climate models (GCMs). Liu et al. (2007) implemented Meyers et al. (1992) in CAM3 and in CAM5 (Gettelman et al., 2010) for the immersion/condensation/deposition mechanisms. Xie et al. (2013) evaluated the DeMott et al. (2010) parameterization in CAM5, in comparison with Meyers et al. (1992). Lohmann and Diehl (2006) implemented the Diehl and Wurzler (2004) parameterization in the global climate model of the Max Planck Institute for Meteorology (ECHAM5) for the immersion freezing of cloud droplets. Hoose

ACPD
14, 7141–7186, 2014

et al. (2010) implemented the CNT in CAM3-Oslo for the immersion, deposition and contact freezing of dust, soot, and biological aerosols. In their paper, they suggest that assuming stochastic ice nucleation with all particles having the same fixed single contact angle, especially with the constant freezing rate in time, can not fit some observations very well. Immersion freezing and deposition nucleation by dust in Hoose et al. (2010) are fitted to the observation data obtained specifically for montmorillonite (Pitter and Pruppacher, 1973) and illite (Zimmermann et al., 2008) respectively. Thus their results may not reflect the ice nucleation behavior by natural dust particles, which are mixtures of complex mineral components.

In this study, we implement the single-α model (Hoose et al., 2010) in CAM5 to represent the heterogeneous ice nucleation of natural dust and BC in mixed-phase clouds. The single-α model is further improved by the α-PDF model to correct the time-dependent behavior of droplet freezing. To better represent the ice nucleation of natural dust found in ambient observations, we use recent observation data on Saharan dust to constrain the parameters used in the CNT parameterization. The model description is presented in Sect. 2. Section 3 describes the CNT parameterizations, with the resulting fitting parameters. In Sect. 4, the model experiments and results are presented. Uncertainties and implications are discussed in Sect. 5.

2 CAM5

CAM5 includes a two-moment stratiform cloud microphysics scheme (Morrison and Gettelman, 2008 (MG08); Gettelman et al., 2008, 2010). This scheme predicts number concentrations and mass mixing ratios of cloud droplets and ice crystals, while the number concentrations and mass mixing ratios of snow and rain are diagnosed. MG08 treats the microphysical conversions among cloud liquid droplets, ice crystals, rain and snow. As for cloud droplet activation, it follows the Abdul-Razzak and Ghan (2000) parameterization. MG08 was further updated in CAM5 (Gettelman et al., 2010) to implement the Liu et al. (2007) scheme for ice crystal nucleation in mixed-phase

ACPD
14, 7141–7186, 2014

and cirrus clouds. In mixed-phase clouds, Meyers et al. (1992) is used for deposition, immersion, and condensation freezing of cloud droplets, which, however, does not provide a link of ice nuclei (IN) number concentration to aerosol properties. In addition, the Young (1974) scheme is used for the contact freezing of cloud droplets by the coarse mode dust.

CAM5 includes a modal aerosol module (MAM) to represent aerosol processes and properties in the atmosphere (Liu et al., 2012a). It predicts aerosol number concentrations and mass mixing ratios of multiple aerosol species in three aerosol modes: Aitken, accumulation and coarse mode. MAM treats major aerosol species including mineral dust, BC, sea salt, sulfate, and primary and secondary organic aerosols. These aerosol species are internally mixed within a single mode, but externally mixed between different modes. Aerosol species in cloud-borne states are also explicitly treated, but not predicted in the model.

The deep convection scheme in CAM5 follows Zhang and McFarlane (1995) but with the dilute Convective Available Potential Energy (CAPE) modification described in Neale et al. (2008). The shallow convection scheme is from Park and Bretherton (2009). The stratus-radiation-turbulence interactions in CAM5 are explicitly simulated by the moist turbulence scheme (Bretherton and Park, 2009). The radiative transfer calculations for aerosol and cloud radiative effects are based on the Rapid Radiative Transfer Model for GCMs (RRTMG) (Iacono et al., 2008).

3 New heterogeneous ice nucleation parameterization in CAM5

3.1 Single contact angle (α) model

In the CNT, ice nucleation is treated as a stochastic process (Pruppacher and Klett, 1997). An energy barrier has to be passed to capture more molecules to small agglomerates of ice (subcritical germs) on the surface of ice nucleus, until a critical germ size is reached. Following the notation in Hoose et al. (2010), both deposition and im-

ACPD
14, 7141–7186, 2014

mersion freezing can be treated in the same general form based on the CNT. Following the suggestion of Chen et al. (2008), we calculate the contact freezing with the critical germ radius of immersion freezing and the homogeneous energy of germ formation of deposition freezing, according to "Cooper's hypothesis" (Cooper, 1974).

We modify the original expression used in Hoose et al. (2010) about J_{het}, the rate of heterogeneous nucleation per aerosol particle and per second, with the form factor (f) raised to the $-1/2$ power instead of $1/2$ (see Eq. 1), due to the unphysical behavior of the original expression which implies that $J_{het} \to 0$ when $f \to 0$ (i.e., the ice nucleation rate will become smaller on more easily wettable materials) (Barahona, 2012; Määttänen et al., 2005).

$$J_{het} = \frac{A' r_N^2}{\sqrt{f}} \exp\left(\frac{-\Delta g^{\#} - f\Delta g_g^o}{kT}\right) \quad (1)$$

where A' is a prefactor, r_N is the aerosol particle radius, f is a form factor containing information about the aerosol's ice nucleation ability, $\Delta g^{\#}$ is the activation energy, Δg_g^o is the homogeneous energy of germ formation, k is the Boltzmann constant, and T is the temperature in K.

The second modification is about f itself. Due to the uncertainty of assuming a spherical substrate (or any other simple geometry) (Barahona, 2012), and the difference between a flat surface and a spherical surface can be ignored when the diameter of particle is larger than 100 nm, we calculate the compatibility parameter f with a flat surface instead of the convex surface. Thus f has the form as (Pruppacher and Klett, 1997)

$$f = \frac{1}{4}(2+m)(1-m)^2 \quad (2)$$

where $m \equiv \cos\alpha$, α is the contact angle.

Except for the above changes, detailed descriptions on the formulation of CNT for the immersion, deposition and contact freezing can be found in Hoose et al. (2010).

ACPD
14, 7141–7186, 2014

We note that Hoose et al. (2010) used the activation fraction of aerosols, which is diagnosed from the droplet activation parameterization, to partition dust and soot number concentrations in each grid into the interstitial portion for the deposition and contact freezing and into the cloud borne portion for the immersion freezing. However, in CAM5 we can directly use the interstitial and cloud borne dust and soot number concentrations in the ice nucleation calculation, since CAM5 explicitly treats these two states of aerosols.

3.2 α-PDF model

We consider the α-PDF model for the immersion freezing by natural dust to replace the single-α model in Hoose et al. (2010). In the α-PDF model, we can take the heterogeneity of individual particles in the aerosol population into account. The particle surface is still uniform in the ice nucleation property for each particle but differs within an ensemble of particle population by a distribution of different contact angles, which are assumed to follow a log-normal probability density function (Marcolli et al., 2007; Lüönd et al., 2010).

The log-normal probability density function which represents the occurrence probability of one contact angle for one particle is given by

$$p(\alpha) = \frac{1}{\alpha\sigma\sqrt{2\pi}} \exp\left(-\frac{(\ln(\alpha) - \ln(\mu))^2}{2\sigma^2}\right) \quad (3)$$

Where μ is the mean contact angle and σ is the standard deviation.

The frozen fraction for a given temperature can then be calculated as

$$f_{\mathrm{act},\alpha\text{-pdf}} = 1 - \int_0^{\pi} p(\alpha) \cdot \exp\left(-J_{\mathrm{imm}}(T,\alpha)\Delta t\right) \mathrm{d}\alpha \quad (4)$$

Here J_{imm} is the immersion nucleation rate for one particle with one certain contact angle, and Δt is the model time step. It should be mentioned that in the global climate

ACPD
14, 7141–7186, 2014

model, the different time dependences of the frozen fraction in the single contact angle model and the α-PDF model are only treated within one time step. In a following time step additional (and unphysical) ice nucleation would also occur with the α-PDF model if temperature is constant. However, due to the long time step of the model, this is probably an acceptable, relatively small artifact (i.e., IN can be refilled during this time step due to the mixing and cloud condensation nuclei (CCN) activation of fresh particles into the cloud).

3.3 Fitting parameters for natural dust and soot

Fitting parameters in the CNT such as the single contact angle (α) and activation energy ($\Delta g^{\#}$) in the single-α model can be derived by minimizing the root mean square error (RMSE) of frozen fractions between observation data and model results. Thus the RMSE is calculated as:

$$\mathrm{RMSE} = \sqrt{\frac{1}{N}\sum_{1}^{N}\left[F_{\mathrm{ice}} - F_{\mathrm{ice}}^{\mathrm{mod}}\right]^2} \tag{5}$$

where F_{ice} is the observed frozen fraction, $F_{\mathrm{ice}}^{\mathrm{mod}}$ is the frozen fraction calculated from the single-α model, and N is total number of observation data points.

The formula to derive uncertain parameters in the α-PDF approach is the same as Eq. (5) except that we calculate $F_{\mathrm{ice}}^{\mathrm{mod}}$ from the α-PDF model. In order to calculate $F_{\mathrm{ice}}^{\mathrm{mod}}$, its integral form of Eq. (4) was discretized into 2000 bins, and then the PDF distribution parameters, standard deviation (σ) and mean contact angle (μ) were iterated to find the best fit following Eq. (5).

The resulting fitting parameters for the immersion and deposition freezing based on the single-α model are listed in Table 1. Observation data for the immersion freezing of dust is obtained from the Colorado State University CFDC-HIAPER version I (CSU CFDC-IH) experiment, which is selected for the relative humidity with respect to water ($\mathrm{RH_w}$) at 106 % (CSU106) (DeMott et al., 2011), and data for the deposition freezing

ACPD
14, 7141–7186, 2014

on dust is from the Koehler et al. (2010)'s laboratory study. Both of the two studies used samples for Saharan dust. The immersion and deposition by soot are still based on the measurements (DeMott, 1990; Möhler et al., 2005) used in Hoose et al. (2010). However due to the modification of some formulas in Sect. 3.1, we refit to these data again.

For the α-PDF model, due to the fact that the activation energy is aerosol, nucleation mode and temperature dependent and is independent on the contact angle (Hoose et al., 2010; Chen et al., 2008; Zobrist et al., 2007), we use the same value for the activation energy as that in the single-α model. The resulting fit parameters from different experiments are listed in Table 2. For the comparison, fit parameters with the single-α model, including CSU106 listed in Table 1, are also given. The experiments were performed over a wide temperature range for Saharan dust sampled in the 2007 International Workshop on Comparing Ice Nucleation Measuring Systems ICIS-2007 (DeMott et al., 2011). These include two experiments of CSU CFDC-IH with 106 % and 108 % RH_w (CSU106 and CSU108, respectively), and three experiments conducted with the Zurich Ice Nuclei Chamber (ZINC) at RH_w of 106 %, 108 % and 110 % (ZINC106, ZINC108, and ZINC110, respectively). It can be seen that the RMSEs with the single-α model in all five experiments are larger than those with the α-PDF model. The reason about this result can be seen from the Fig. 1, which shows the observation data from CSU106 and ZINC106, and their fits with the single-α model and the α-PDF model. The α-PDF model reproduces the slow decrease of active fraction with the increase of temperature and makes a better agreement with observation data points at warm temperatures ($T > -20\,^{\circ}C$) while the single-α model leads to a steep decrease of active fraction with the increase of temperature and thus results in large errors at warm temperatures. Therefore, larger RMSEs with the single-α model are mainly from its fit at warm temperatures.

ACPD
14, 7141–7186, 2014

4 Results

A control experiment (CTL) with the default freezing parameterization in CAM5 (Meyers et al., 1992), an experiment based on the CNT in Hoose et al. (2010) (single-α), an experiment with the new α-PDF model as described above, and several sensitivity experiments with the α-PDF model have been carried out (see Table 3). The sensitivity experiments are designed to explore the sensitivities of model simulations to the mean contact angle and standard deviation in the α-PDF model. The mean contact angle is changed by $\pm 15^{\circ}$ (in order to include 61°, which is the fit result from the ZINC measurements), and standard deviation increased by 4 and 8 times in these sensitivity experiments.

All these simulations are run for 6 years with the model configuration of $1.9^{\circ} \times 2.5^{\circ}$ and 30 levels, using prescribed sea surface temperatures (SST) and sea ice extent. The aerosol input uses the online aerosol model, MAM3. The last 5 year results are used in the analysis.

4.1 Particle number concentrations

The zonal and annual mean number concentrations of interstitial, cloud borne and total (interstitial plus cloud borne) mineral dust and soot particles are shown in Fig. 2. As is shown in Fig. 2, the magnitudes of interstitial dust and soot number concentrations are about one order of magnitude larger than those of cloud borne ones. In cloud borne aerosols, there are more dust particles than soot particles, which is an important point to explain the dominant role of dust in heterogeneous freezing compared to soot. The maximum number concentration of interstitial soot, internally mixed in the accumulation mode, is near the surface in the Northern Hemisphere (NH), exceeding $50\,\mathrm{cm}^{-3}$ in the zonal mean. Interstitial mineral dust particles in the accumulation and coarse mode, reach $10–50\,\mathrm{cm}^{-3}$ in the sub-tropics and at the surface of NH ($\sim 30^{\circ}$ N). Interstitial mineral dust and soot are uplifted from their source regions to the middle and upper troposphere and transported to the Arctic in the upper troposphere (Liu et al., 2012b).

ACPD
14, 7141–7186, 2014

The total number concentrations of these two species are mainly from their interstitial particles. As noted above, cloud borne aerosols are used as an input for the immersion freezing, while interstitial aerosols (only the uncoated portion showed in Fig. 3) are used as an input for deposition and contact freezing. Compared to Hoose et al. (2010), the total number concentration of soot is one order of magnitude lower in CAM5, which can be attributed to the different size distributions used for soot in two models (CAM5 and CAM3-Oslo). In the CAM3-Oslo model, soot is emitted into both the nucleation (initial diameter: 0.024 µm), the Aitken (initial diameter: 0.08 µm) and accumulation (initial diameter: 0.2 µm) modes (Seland et al., 2008). Its number concentration is dominated by uncoated nucleation and Aitken mode particles, which contribute to the higher number concentration, while in CAM5 soot is emitted in the accumulation mode with a larger emission size (0.08 µm in diameter). Dust number concentrations in CAM5 are mainly from the accumulation mode with the diameter range of 0.1–1.0 µm, while coarse mode number concentration is one order of magnitude lower (Liu et al., 2012a). A similar ratio between accumulation and coarse mode dust is also found in CAM3-Oslo.

The interstitial mineral dust and soot particles are further divided into two categories: coated and uncoated particles. The number concentrations of them are derived from the coated fraction f_{coated}, which is calculated by distributing the soluble mass (sulfate and organic) over the soot and dust cores in the internally mixed modes, requiring a minimum coverage of one monolayer. Suppression of heterogeneous ice nucleation is dependent on coating thickness or the fractional soluble mass coverage. Generally we assume that if a potential IN is covered by more than one monolayer, its heterogeneous nucleation behavior in the deposition and contact modes will be suppressed completely due to a shift to the higher onset relative humidity with respect to ice, RHi, and to the colder onset temperature (Hoose et al., 2010; Möhler et al., 2008). Therefore, only those uncoated particles will participate in ice nucleation. The number concentrations of coated and uncoated interstitial aerosol particles are shown in Fig. 3. It can be seen that the uncoated dust number concentration is several orders of magnitude lower than that of coated dust particles, with the criteria of one monolayer coating by

ACPD
14, 7141–7186, 2014

soluble aerosol species. Compared to dust, nearly all the soot particles are coated (the concentration of the uncoated soot particles is smaller than $10^{-6}\,cm^{-3}$). This is because soot cores have the smaller sizes than dust cores and soot is directly emitted into the accumulation mode in MAM3. If soot is directly emitted into the primary carbon mode (e.g., MAM4 or MAM7), which is the insoluble mode, there should be much more uncoated soot particles, especially with slow aging of the primary carbon mode (not shown in this paper). However, as compared to dust, soot is a much less efficient IN and immersion freezing is the dominant process (see Sect. 4.2), it won't have large effects on the total nucleated ice number concentrations even using MAM4 or MAM7.

4.2 Ice nucleation rates

The zonal and annual mean rates of immersion, deposition, and contact freezing ($\Delta N_i/\Delta t$, here ΔN_i is the ice crystal number concentration change over one model time step Δt (30 min); note that it is different from J_{het}) by dust and soot in the PDF simulation are shown in Fig. 4. It can be seen that the immersion freezing by dust is the dominant ice nucleation mechanism, which is consistent with Hoose et al. (2010), followed by soot immersion, dust deposition, and dust contact freezing. Recent observations (de Boer et al., 2011) also indicated that immersion freezing may be the dominant freezing mechanism in mixed-phase clouds, compared to other freezing modes (deposition freezing and contact freezing). This was concluded from the observation that liquid droplets occurred prior to the ice formation in mixed-phase clouds, which was also detected by Ansmann et al. (2008). A recent laboratory study by Bunker et al. (2012) found that hundreds of collisions of mineral dust particles with a supercooled droplet are needed to initiate the contact freezing. Thus the contact freezing might not be a dominant ice formation pathway in mixed-phase clouds. The other two nucleation modes by soot (i.e., soot deposition and soot contact) are nearly negligible, because the number concentration of uncoated interstitial soot particles is very small (see Fig. 3). In general, the ice nucleation rates peak over the regions where dust and soot particles are emitted. It should be noted here that freezing rates appear larger

ACPD
14, 7141–7186, 2014

than 0 at $T > 0\,^{\circ}\mathrm{C}$ is due to the zonal and annual averaging. The vertically integrated and globally averaged nucleation rates in the PDF simulation are shown in Fig. 5. The relative roles of all these rates in mixed-phase clouds can be seen more clearly. The freezing rates by dust are similar to those of Hoose et al. (2010). However, the freezing rates by soot are much smaller because of the large differences in the simulated soot number concentrations between two models (CAM5 and CAM-Oslo) as well as the internal mixture of soot in the accumulation mode assumed in CAM5 (Sect. 4.1), which leads to smaller ice nucleation rates in CAM5. In CAM-Oslo, a larger fraction of the soot particles are uncoated and can thus contribute to deposition and contact nucleation, which we do not consider realistic, in particular as these two processes are not observed at warm subzero temperatures in laboratory experiments.

For the comparison, the immersion freezing by dust simulated by the single-α model (CNT) is shown in Fig. 6. We can see that compared to the single-α model, ice nucleation simulated by the α-PDF model (see Fig. 4) can occur at lower altitudes (with warmer temperatures), which is attributed to the PDF distribution of contact angles in the α-PDF model. It means that particles with smaller contact angles in the α-PDF model can nucleate at warmer temperatures where the particles with the same mean contact angles can not nucleate. Generally, the major increase of immersion freezing in the PDF simulation, compared to the CNT simulation, occurs at warm subzero temperatures due to its PDF distribution of contact angles.

4.3 Occurrence frequency of ice nucleation modes

In order to count the different ice nucleation events, we follow the same method as that in Liu et al. (2012b), which counts the homogeneous ice nucleation and heterogeneous ice nucleation events in cirrus clouds when there are new nucleated ice number concentrations from these two ice nucleation modes respectively. Therefore, in this study, only when the freezing rate ($\Delta N_{\mathrm{i}}/\Delta t$) from one ice nucleation mode is larger than 0, then we count this ice nucleation event. The occurrence frequency of immersion freezing, deposition nucleation and contact nucleation as a function of temperature from the

ACPD
14, 7141–7186, 2014

PDF simulation and the frequency of immersion freezing from the CNT simulation are shown in Fig. 7. All the data in each temperature bin (2 K) are shown with the whiskers indicating the 5th and 95th percentiles, and with the boxes indicating the 25th and 75th percentiles and the median. The occurrence frequencies for a period of 5 years (monthly data) are output between −90° S to 90° N and from 1000 hPa to 500 hPa. It is obvious to see that the frequency of immersion freezing is about three orders of magnitude higher than contact nucleation and deposition nucleation, both of which have the similar magnitude. The frequency of deposition nucleation and contact nucleation are not obviously dependent on temperature, which is similar to the weak temperature dependences of the nucleation rates of these two nucleation modes in Hoose et al. (2010) (see Fig. 2 in their paper). The frequency of immersion freezing in the PDF simulation at warmer temperatures ($T > 265$ K) is much higher than that in the CNT simulation.

Figure 8 shows the zonal and annual mean frequency distribution of immersion freezing, deposition nucleation and contact nucleation. The pattern of immersion freezing is different from the two other modes. There are two maximum centers located in the polar regions. The deposition and contact nucleation peak over the source regions at 30° N–60° N and 20° S–40° S. It is because dust and soot near the source regions are uncoated, leading to occurrence of the deposition and contact nucleation. When these particles age and are coated in the process of uplifting and transporting to polar regions, the deposition and contact nucleation become even less important and conversely immersion freezing dominates. The frequency of immersion freezing after introducing the α-PDF model (PDF) compared to the single-α model (CNT) is increased, especially at lower altitudes (with warmer temperatures).

4.4 Sensitivity tests with the α-PDF model

Figure 9 shows the effects of changes of the uncertain parameters in the α-PDF model on active fraction with temperature. Figure 9a shows the impact of mean contact angle. It's obvious that with the decrease of the mean contact angle, the active fraction increases, making the curve shift upwards. However, the temperature range in which the

ACPD
14, 7141–7186, 2014

rapid increase of the active fraction does not become broader, indicating that changes of the mean contact angle don't have impact on the temperature dependence of the active fraction. Instead in Fig. 9b, the temperature dependence of the active fraction changes with the change of the standard deviation. Increasing the standard deviation, which makes larger heterogeneity among the particle population, enlarges the temperature range of the rapid increase of active fraction, leading to the stronger temperature dependence and thus weaker time dependence (Niedermeier et al., 2011; Welti et al., 2012). Though the magnitude of changes of active fraction due to the change of the standard deviation is much smaller than that due to the mean contact angle, it results in the transition of the freezing behavior, from the stochastic behavior to the singular behavior (Niedermeier et al., 2011, 2013). Some variances of cloud properties with the changes of these uncertain parameters in the α-PDF model will be shown in Sect. 4.6.

4.5 Comparison of IN concentrations with observations

Currently the mostly used instrument for detecting IN concentrations in the atmosphere is the continuous-flow diffusion chamber (CFDC) (Rogers et al., 2001), which allows interstitial aerosol particles to enter through an inlet and to expose a specific temperature and/or humidity in the chamber. Then the number concentration of ice crystals nucleated in the chamber after a residence time of 5–20 s is counted. We calculate modeled IN concentrations and compare them with CFDC observations. The calculation uses modeled interstitial aerosol concentrations which are sampled at the same locations and pressures as observations and with the same processing temperatures as operated in the CFDC. We note that when comparing to observations we only consider the immersion and deposition freezing because the residence time in CFDC is short and thus its technique can not directly assess whether aerosols particles are active as contact freezing nuclei (DeMott et al., 2010).

Both the single-α and α-PDF models are time dependent, and CFDC has a residence time of approximate 10 s, so we define the modeled IN number concentration (hereafter termed "model IN(10 s)") as a 10 s integral over the freezing rate ($\Delta N_i/\Delta t$),

ACPD
14, 7141–7186, 2014

following Hoose et al. (2010). Figure 10 shows the model IN(10 s) concentrations in two simulations (CNT and PDF), which are sampled at the grid boxes including the CFDC measurement locations and at the same pressure level as field observations. The magnitude of model IN(10 s) concentrations simulated by CNT and PDF are similar as observations except for Barrow, Alaska (some data points which are clearly below the acceptable minimum detection limit of CFDC are removed). At warmer temperatures ($T > -20\,^{\circ}$C) model IN(10 s) concentrations simulated by the PDF simulation at Colorado region from winter icing in storms project in 1994 (WISP94) in February and at Storm Peak in April/May agree with observations better than those by CNT in which the simulated IN(10 s) concentrations are several orders of magnitude smaller than observations. The modeled weak temperature dependence at $T > -20\,^{\circ}$C in Colorado region in the PDF simulation is confirmed by observations, where there is an indication for trend to be flatter (the observation data in Lüönd et al. (2010) also has this trend at warm temperatures). Conversely, when the temperature is warmer than $-20\,^{\circ}$C, the IN(10 s) concentrations simulated by the CNT simulation reduce rapidly, resulting in several orders of magnitude discrepancy with observations (see Fig. 10a and c). Due to the rapid decrease of the IN(10 s) concentrations in the CNT simulation, the magnitude of the IN(10 s) concentrations becomes smaller than the y-axis min value, which causes CNT data not to be shown in the Fig. 10a. The temperature variation of model IN(10 s) concentrations in the CNT and PDF simulations become flat at $T < -25\,^{\circ}$C at Storm Peak, which is consistent with the observations. The model IN(10 s) concentrations at Barrow, Alaska in the CNT and PDF simulations are both one or two orders of magnitude smaller than observations. This may be due to the fact that the simulated number concentrations of aerosol particles (e.g., soot) in Arctic are one or two orders of magnitude smaller than observations (Liu et al., 2012a; Wang et al., 2011).

For a more detailed comparison at warm temperature regions, spatial distributions of model IN(10 s) concentrations from the simulation PDF are shown in Fig. 11 with some field measurements of IN concentrations around the globe (DeMott et al. (2010), Central USA, 239 K $< T <$ 246 K and 241 K $< T <$ 258 K; Rosinski et al. (1987), Cen-

ACPD
14, 7141–7186, 2014

tral Pacific, 254 K < T < 270 K; Rosinski et al. (1995), East China Sea, T = 253 K; Bigg et al. (1973), South of Australia, T = 258 K). In the East China Sea, Brazil and Central USA regions, as there is only one single field campaign at each region (i.e., only one single circle at each region in the Fig. 11) and their colors are similar as the background colors of modeled IN(10 s) concentrations, we utilize darkgreen rectangles to highlight them for seeing them clearly. The model IN(10 s) concentrations are selected for four specific temperatures which fall into the corresponding range of observed temperatures as specified in each plot. All the field measurements are located on surface, and thus we also use interstitial aerosol concentrations at surface as input to diagnosed IN concentrations. It can be seen that the model IN(10 s) concentrations are in agreement with observations, especially at East China Sea, Brazil and Central USA. As for comparison with observations at South Australia, most of colored circles match the background colors well except for few several circles where a biogenic source of IN may play a dominant role in determining IN concentrations in near-surface-air (Burrows et al., 2013). Therefore, from Figs. 10 and 11, the α-PDF model enhances the IN concentrations at warmer temperatures and agrees well with observations, which can be attributed to a distribution of contact angles.

Georgii and Kleinjung (1967) found that IN number concentrations correlate well with the number concentration of coarse mode aerosol particles but not with the total aerosol number concentration, which is dominated by smaller particles. More recent IN measurements with the CFDC obtained the similar results (DeMott et al., 2006, 2010, 2014). Figure 12 shows the model IN(10 s) concentrations in the CNT and PDF simulations as a function of number concentrations of aerosols with diameter larger than 0.5 µm (Na_{500}), sampling at T = −21 °C (Fig. 12a and b) which is the temperature used in the observations (DeMott et al., 2006; Georgii and Kleinjung, 1967) and sampling at T = −27 °C (Fig. 12c and d) to compare with DeMott et al. (2014) with the same processing temperature. In CAM5, we sample Na_{500} as follows: dust number concentration in the accumulation mode with the diameter larger than 0.5 µm is calculated with predicted dust mass mixing ratio in this mode and prescribed size distribution for trans-

ACPD
14, 7141–7186, 2014

ported dust (Zender et al., 2003). Dust number concentration in the coarse mode is calculated from the predicted total number concentration in the coarse mode weighted by the mass fraction of dust in this mode. Then we use these two dust number concentration as the Na_{500}. We neglect the contribution of soot and sea salt to Na_{500}, due to its smaller size. In Fig. 12a and b, for both the CNT and PDF simulations, almost all dots locate in-between the two power-law fits by DeMott et al. (2006) and Georgii and Kleinjung (1967). Compared to the CNT simulation, the model IN(10 s) concentrations simulated from the PDF simulation shift a little upwards. In order to compare with DeMott et al. (2014), we convert modeled Na_{500} and IN(10 s) to those at standard temperature and pressure conditions and the results are shown in Fig. 12c and d. Both in the CNT and PDF simulations, the magnitude of the model IN(10 s) concentrations are at and around the DeMott et al. (2014) proposed parameterization (solid red line), thus yielding excellent agreement. The DeMott et al. (2014) parameterization, developed from the DeMott et al. (2010) parameterization to account for additional aerosol compositional dependencies, is for the dust ice nuclei exclusively. For atmospheric application, an additional correction factor is introduced to account for the underestimate of the immersion freezing fraction of mineral dust particles for CFDC data. Their parameterization reflects the mineral dust data from the Saharan or Asian regions very well and indicates they can be parameterized as a common particle type for global modeling. Therefore, the atmospheric application of our parameterization based on Saharan dust is successfully confirmed by DeMott et al. (2014).

4.6 Aerosol indirect forcing

Table 4 lists the global and annual mean cloud and radiative properties for the present-day simulations and differences of these variables between the present-day and preindustrial simulations. As for the present-day experiments, with the implementation of two stochastic heterogeneous ice nucleation parameterizations, the global mean ice water path (IWP) decreases for the CNT and all the PDF simulations compared to the CTL simulation due to fewer nucleated ice crystals in the CNT and PDF simulations. This

ACPD
14, 7141–7186, 2014

can be confirmed from the comparison of the vertically integrated column ice crystal number concentration (ICENUM) in mixed-phase clouds ($-37\,^{\circ}\mathrm{C} < T < 0\,^{\circ}\mathrm{C}$) among different simulations. The CTL simulation has the largest ICENUM in mixed-phase clouds. As a consequence, the CNT and all the PDF simulations exhibit larger global mean liquid water path (LWP) than that in the CTL simulation. This is because fewer ice crystals slow down Wegener–Bergeron–Findeisen process, and thus increase the liquid water content. The larger (smaller) mean contact angle with the smaller (larger) active fraction in MU1 (MU2) in the PDF sensitivity simulations results in smaller (larger) IWP and ICENUM in the mixed-phase clouds.

The LWP and IWP changes between present-day and pre-industry in the CTL simulation are $3.26\,\mathrm{g\,m^{-2}}$ and $0.14\,\mathrm{g\,m^{-2}}$ respectively, while those in the CNT and PDF simulations are much larger, especially the IWP change. Larger changes of IWP and LWP between present-day and pre-industry in the CNT and PDF simulations lead to larger changes of shortwave cloud forcing (SWCF) and longwave cloud forcing (LWCF). The SWCF change differs by $0.38\,\mathrm{W\,m^{-2}}$ and LWCF change by $0.32\,\mathrm{W\,m^{-2}}$ between the CTL and CNT simulations ($0.22\,\mathrm{W\,m^{-2}}$ and $0.31\,\mathrm{W\,m^{-2}}$ between the CTL and PDF simulations respectively), although the net cloud forcing change differs by less than $0.1\,\mathrm{W\,m^{-2}}$. The changes of total cloud cover (TCC), low-cloud cover (LCC) and integrated column ice crystal number concentration (ICENUM) in the mixed-phase clouds between present-day and pre-industry are also larger in the CNT and PDF simulations than those in the CTL simulation.

5 Conclusions

A classical-nucleation-theory-based parameterization of heterogeneous ice nucleation is implemented in CAM5 based on Hoose et al. (2010). In addition, we make further improvements by introducing a probability distribution of contact angles for the freezing process by natural dust. We fit the uncertain parameters of the single-α and the α-PDF models to laboratory data for natural dust and BC (soot). Compared to the single-α

ACPD
14, 7141–7186, 2014

model, the α-PDF model has a better agreement with observations at warmer temperatures by enhancing the IN number concentrations and further results in weaker temperature and time dependence of IN number concentration. Therefore, ice crystals can form at lower altitudes (with warmer temperatures) from the α-PDF model than the single-α model. On the other hand, the α-PDF model alleviates the conflict with observations, especially for the assumption in the single-α model that the freezing rate is constant with time.

From the sensitivity experiments with the α-PDF model, we find that the change of mean contact angle has a larger impact on the active fraction than that of standard deviation, which is consistent with the cloud-resolving model results by Kulkarni et al. (2012). When increasing (reducing) the mean contact angle, the active fraction will decrease (increase). Meanwhile, the increase of standard deviation will lead to a transition of the nucleation behavior: from stochastic behavior to singular behavior. Once approaching to the singular behavior, further effects of the increase of standard deviation on the freezing rate may be depressed. Immersion freezing by natural dust in both single-α and α-PDF models is the dominant nucleation mechanism in mixed-phase clouds, consistent with Hoose et al. (2010).

More studies are needed to further investigate the transition between the stochastic behavior and the deterministic behavior of heterogeneous ice nucleation in global models in the future. As the model time step (30 min) is large for the stochastic ice nucleation behavior and the nucleation rate should not be constant in a model time step, we may need to set sub-time steps and take ice-borne aerosols (i.e., the nucleation scavenging of the IN during one sub-time step) into account to further investigate the time dependence in the global model. Other stochastic models like the active site model and the soccer ball model (Niedermeier et al., 2013) should be implemented and their behaviors explored in global models.

Acknowledgements. We would like to thank P. J. DeMott for providing the CFDC data shown in Figs. 10 and 11. This research was supported by the Office of Science of the US Department of Energy (DOE) as part of the Earth System Modeling Program. We would like to acknowledge

ACPD
14, 7141–7186, 2014

the use of computational resources (ark:/85065/d7wd3xhc) at the NCAR-Wyoming Supercomputing Center provided by the National Science Foundation and the State of Wyoming, and supported by NCAR's Computational and Information Systems Laboratory. CH acknowledges funding by the Helmholtz Association through the President's Initiative and Networking Fund and by the Deutsche Forschungsgemeinschaft through project FOR 1525.

References

Abdul-Razzak, H. and Ghan, S. J.: A parameterization of aerosol activation: 2. Multiple aerosol types, J. Geophys. Res.-Atmos., 105, 6837–6844, doi:10.1029/1999JD901161, 2000.

Ansmann, A., Tesche, M., Althausen, D., Müller, D., Seifert, P., Freudenthaler, V., Heese, B., Wiegner, M., Pisani, G., Knippertz, P., and Dubovik, O.: Influence of Saharan dust on cloud glaciation in southern Morocco during the Saharan Mineral Dust Experiment, J. Geophys. Res.-Atmos., 113, D04210, doi:10.1029/2007JD008785, 2008.

Barahona, D.: On the ice nucleation spectrum, Atmos. Chem. Phys., 12, 3733–3752, doi:10.5194/acp-12-3733-2012, 2012.

Bigg, E. K.: The formation of atmospheric ice crystals by the freezing of droplets, Q. J. Roy. Meteor. Soc., 79, 510–519, doi:10.1002/qj.49707934207, 1953.

Bigg, E. K.: Ice nucleus concentrations in remote areas, J. Atmos. Sci., 30, 1153–1157, doi:10.1175/1520-0469(1973)030<1153:INCIRA>2.0.CO;2, 1973.

Bretherton, C. S. and Park, S.: A new moist turbulence parameterization in the community atmosphere model, J. Climate, 22, 3422–3448, doi:10.1175/2008JCLI2556.1, 2009.

Bunker, K. W., China, S., Mazzoleni, C., Kostinski, A., and Cantrell, W.: Measurements of ice nucleation by mineral dusts in the contact mode, Atmos. Chem. Phys. Discuss., 12, 20291–20309, doi:10.5194/acpd-12-20291-2012, 2012.

Burrows, S. M., Hoose, C., Pöschl, U., and Lawrence, M. G.: Ice nuclei in marine air: biogenic particles or dust?, Atmos. Chem. Phys., 13, 245–267, doi:10.5194/acp-13-245-2013, 2013.

Chen, J.-P., Hazra, A., and Levin, Z.: Parameterizing ice nucleation rates using contact angle and activation energy derived from laboratory data, Atmos. Chem. Phys., 8, 7431–7449, doi:10.5194/acp-8-7431-2008, 2008.

Cooper, W. A.: A possible mechanism for contact nucleation, J. Atmos. Sci., 31, 1832–1837, doi:10.1175/1520-0469(1974)031<1832:APMFCN>2.0.CO;2, 1974.

ACPD
14, 7141–7186, 2014

de Boer, G., Morrison, H., Shupe, M. D., and Hildner, R.: Evidence of liquid dependent ice nucleation in high-latitude stratiform clouds from surface remote sensors, Geophys. Res. Lett., 38, L01803, doi:10.1029/2010GL046016, 2011.

DeMott, P. J.: An exploratory study of ice nucleation by soot aerosols, J. Appl. Meteorol., 29, 1072–1079, doi:10.1175/1520-0450(1990)029<1072:AESOIN>2.0.CO;2, 1990.

DeMott, P. J., Cziczo, D. J., Prenni, A. J., Murphy, D. M., Kreidenweis, S. M., Thomson, D. S., Borys, R., and Rogers, D. C.: Measurements of the concentration and composition of nuclei for cirrus formation, P. Natl. Acad. Sci. USA, 100, 14655–14660, doi:10.1073/pnas.2532677100, 2003.

DeMott, P. J., Prenni, A. J., Richardson, M. S., Kreidenweis, S. M., Twohy, C. H., and Rogers, D. C.: Ice nuclei variability, relation to ambient aerosol properties, and impacts on mixed-phase clouds. Preprints, 12th Conf. on Cloud Physics, Madison, WI, Amer. Meteor. Soc., 2.1, 10 July 2006, available at: http://ams.confex.com/ams/Madison2006/techprogram/paper_113242.htm, 2006.

DeMott, P. J., Prenni, A. J., Liu, X., Kreidenweis, S. M., Petters, M. D., Twohy, C. H., Richardson, M. S., Eidhammer, T., and Rogers, D. C.: Predicting global atmospheric ice nuclei distributions and their impacts on climate, P. Natl. Acad. Sci. USA, 107, 11217–11222, doi:10.1073/pnas.0910818107, 2010.

DeMott, P. J., Möhler, O., Stetzer, O., Vali, G., Levin, Z., Petters, M. D., Murakami, M., Leisner, T., Bundke, U., Klein, H., Kanji, Z. A., Cotton, R., Jones, H., Benz, S., Brinkmann, M., Rzesanke, D., Saathoff, H., Nicolet, M., Saito, A., Nillius, B., Bingemer, H., Abbatt, J., Ardon, K., Ganor, E., Georgakopoulos, D. G., and Saunders, C.: Resurgence in ice nuclei measurement research, B. Am. Meteorol. Soc., 92, 1623–1635, doi:10.1175/2011BAMS3119.1, 2011.

DeMott, P. J., Prenni, A. J., McMeeking, G. R., Sullivan, R. C., Petters, M. D., Tobo, Y., Niemand, M., Möhler, O., Snider, J. R., and Kreidenweis, S. M.: A parameterization of freezing nucleation by mineral dust particles, Atmos. Chem. Phys., in preparation, 2014.

Diehl, K. and Wurzler, S.: Heterogeneous drop freezing in the immersion mode: model calculations considering soluble and insoluble particles in the drops, J. Atmos. Sci., 61, 2063–2072, doi:10.1175/1520-0469(2004)061<2063:HDFITI>2.0.CO;2, 2004.

Georgii, H. and Kleinjung, E.: Relations between the chemical composition of atmospheric aerosol particles and the concentration of natural ice nuclei, J. Rech. Atmos., 3, 145–156, 1967.

ACPD
14, 7141–7186, 2014

Gettelman, A., Morrison, H., and Ghan, S. J.: A new two-moment bulk stratiform cloud microphysics scheme in the Community Atmosphere Model, Version 3 (CAM3). Part II: Single-column and global results, J. Climate, 21, 3660–3679, doi:10.1175/2008JCLI2116.1, 2008.
Gettelman, A., Liu, X., Ghan, S. J., Morrison, H., Park, S., Conley, A. J., Klein, S. A., Boyle, J., Mitchell, D. L., and Li, J. L. F.: Global simulations of ice nucleation and ice supersaturation with an improved cloud scheme in the Community Atmosphere Model, J. Geophys. Res.-Atmos., 115, D18216, doi:10.1029/2009JD013797, 2010.
Hoose, C. and Möhler, O.: Heterogeneous ice nucleation on atmospheric aerosols: a review of results from laboratory experiments, Atmos. Chem. Phys., 12, 9817–9854, doi:10.5194/acp-12-9817-2012, 2012.
Hoose, C., Lohmann, U., Erdin, R., and Tegen, I.: The global influence of dust mineralogical composition on heterogeneous ice nucleation in mixed-phase clouds, Environ. Res. Lett., 3, 025003, doi:10.1088/1748-9326/3/2/025003, 2008.
Hoose, C., Kristjánsson, J. E., Chen, J.-P., and Hazra, A.: A classical-theory-based parameterization of heterogeneous ice nucleation by mineral dust, soot, and biological particles in a global climate model, J. Atmos. Sci., 67, 2483–2503, doi:10.1175/2010JAS3425.1, 2010.
Iacono, M. J., Delamere, J. S., Mlawer, E. J., Shephard, M. W., Clough, S. A., and Collins, W. D.: Radiative forcing by long-lived greenhouse gases: calculations with the AER radiative transfer models, J. Geophys. Res.-Atmos., 113, D13103, doi:10.1029/2008JD009944, 2008.
Knopf, D. A. and Koop, T.: Heterogeneous nucleation of ice on surrogates of mineral dust, J. Geophys. Res.-Atmos., 111, D12201, doi:10.1029/2005JD006894, 2006.
Koehler, K. A., Kreidenweis, S. M., DeMott, P. J., Petters, M. D., Prenni, A. J., and Möhler, O.: Laboratory investigations of the impact of mineral dust aerosol on cold cloud formation, Atmos. Chem. Phys., 10, 11955–11968, doi:10.5194/acp-10-11955-2010, 2010.
Kulkarni, G., Fan, J., Comstock, J. M., Liu, X., and Ovchinnikov, M.: Laboratory measurements and model sensitivity studies of dust deposition ice nucleation, Atmos. Chem. Phys., 12, 7295–7308, doi:10.5194/acp-12-7295-2012, 2012.
Langham, E. and Mason, B.: The heterogeneous and homogeneous nucleation of supercooled water, P. Roy. Soc. Lond. A Mat., 247, 493–504, 1958.
Liu, X. and Penner, J. E.: Ice nucleation parameterization for global models, Meteorol. Z., 14, 499–514, doi:10.1127/0941-2948/2005/0059, 2005.

ACPD
14, 7141–7186, 2014

Liu, X., Penner, J. E., Ghan, S. J., and Wang, M.: Inclusion of ice microphysics in the NCAR Community Atmospheric Model Version 3 (CAM3), J. Climate, 20, 4526–4547, doi:10.1175/JCLI4264.1, 2007.

Liu, X., Easter, R. C., Ghan, S. J., Zaveri, R., Rasch, P., Shi, X., Lamarque, J.-F., Gettelman, A., Morrison, H., Vitt, F., Conley, A., Park, S., Neale, R., Hannay, C., Ekman, A. M. L., Hess, P., Mahowald, N., Collins, W., Iacono, M. J., Bretherton, C. S., Flanner, M. G., and Mitchell, D.: Toward a minimal representation of aerosols in climate models: description and evaluation in the Community Atmosphere Model CAM5, Geosci. Model Dev., 5, 709–739, doi:10.5194/gmd-5-709-2012, 2012a.

Liu, X., Shi, X., Zhang, K., Jensen, E. J., Gettelman, A., Barahona, D., Nenes, A., and Lawson, P.: Sensitivity studies of dust ice nuclei effect on cirrus clouds with the Community Atmosphere Model CAM5, Atmos. Chem. Phys., 12, 12061–12079, doi:10.5194/acp-12-12061-2012, 2012b.

Lohmann, U. and Diehl, K.: Sensitivity studies of the importance of dust ice nuclei for the indirect aerosol effect on stratiform mixed-phase clouds, J. Atmos. Sci., 63, 968–982, doi:10.1175/JAS3662.1, 2006.

Lüönd, F., Stetzer, O., Welti, A., and Lohmann, U.: Experimental study on the ice nucleation ability of size-selected kaolinite particles in the immersion mode, J. Geophys. Res.-Atmos., 115, D14201, doi:10.1029/2009JD012959, 2010.

Määttänen, A., Vehkamäki, H., Lauri, A., Merikallio, S., Kauhanen, J., Savijärvi, H., and Kulmala, M.: Nucleation studies in the Martian atmosphere, J. Geophys. Res.-Planet., 110, E02002, doi:10.1029/2004JE002308, 2005.

Marcolli, C., Gedamke, S., Peter, T., and Zobrist, B.: Efficiency of immersion mode ice nucleation on surrogates of mineral dust, Atmos. Chem. Phys., 7, 5081–5091, doi:10.5194/acp-7-5081-2007, 2007.

Meyers, M. P., DeMott, P. J., and Cotton, W. R.: New primary ice-nucleation parameterizations in an explicit cloud model, J. Appl. Meteorol., 31, 708–721, doi:10.1175/1520-0450(1992)031<0708:NPINPI>2.0.CO;2, 1992.

Möhler, O., Büttner, S., Linke, C., Schnaiter, M., Saathoff, H., Stetzer, O., Wagner, R., Krämer, M., Mangold, A., Ebert, V., and Schurath, U.: Effect of sulfuric acid coating on heterogeneous ice nucleation by soot aerosol particles, J. Geophys. Res.-Atmos., 110, D11210, doi:10.1029/2004JD005169, 2005.

ACPD
14, 7141–7186, 2014

Möhler, O., Field, P. R., Connolly, P., Benz, S., Saathoff, H., Schnaiter, M., Wagner, R., Cotton, R., Krämer, M., Mangold, A., and Heymsfield, A. J.: Efficiency of the deposition mode ice nucleation on mineral dust particles, Atmos. Chem. Phys., 6, 3007–3021, doi:10.5194/acp-6-3007-2006, 2006.

Möhler, O., Benz, S., Saathoff, H., Schnaiter, M., Wagner, R., Schneider, J., Walter, S., Ebert, V., and Wagner, S.: The effect of organic coating on the heterogeneous ice nucleation efficiency of mineral dust aerosols, Environ. Res. Lett., 3, 025007, doi:10.1088/1748-9326/3/2/025007, 2008.

Morrison, H. and Gettelman, A.: A new two-moment bulk stratiform cloud microphysics scheme in the Community Atmosphere Model, Version 3 (CAM3). Part I: Description and numerical tests, J. Climate, 21, 3642–3659, doi:10.1175/2008JCLI2105.1, 2008.

Murray, B., O'Sullivan, D., Atkinson, J., and Webb, M.: Ice nucleation by particles immersed in supercooled cloud droplets, Chem. Soc. Rev., 41, 6519–6554, 2012.

Neale, R. B., Richter, J. H., and Jochum, M.: The impact of convection on ENSO: from a delayed oscillator to a series of events, J. Climate, 21, 5904–5924, 2008.

Niedermeier, D., Hartmann, S., Shaw, R. A., Covert, D., Mentel, T. F., Schneider, J., Poulain, L., Reitz, P., Spindler, C., Clauss, T., Kiselev, A., Hallbauer, E., Wex, H., Mildenberger, K., and Stratmann, F.: Heterogeneous freezing of droplets with immersed mineral dust particles – measurements and parameterization, Atmos. Chem. Phys., 10, 3601–3614, doi:10.5194/acp-10-3601-2010, 2010.

Niedermeier, D., Shaw, R. A., Hartmann, S., Wex, H., Clauss, T., Voigtländer, J., and Stratmann, F.: Heterogeneous ice nucleation: exploring the transition from stochastic to singular freezing behavior, Atmos. Chem. Phys., 11, 8767–8775, doi:10.5194/acp-11-8767-2011, 2011.

Niedermeier, D., Ervens, B., Clauss, T., Voigtländer, J., Wex, H., Hartmann, S., and Stratmann, F.: A computationally efficient description of heterogeneous freezing: a simplified version of the Soccer ball model, Geophys. Res. Lett., 2013, GL058684, doi:10.1002/2013GL058684, 2013.

Niemand, M., Möhler, O., Vogel, B., Vogel, H., Hoose, C., Connolly, P., Klein, H., Bingemer, H., DeMott, P., Skrotzki, J., and Leisner, T.: A particle-surface-area-based parameterization of immersion freezing on desert dust particles, J. Atmos. Sci., 69, 3077–3092, doi:10.1175/JAS-D-11-0249.1, 2012.

ACPD
14, 7141–7186, 2014

Park, S. and Bretherton, C. S.: The University of Washington Shallow Convection and moist turbulence schemes and their impact on climate simulations with the Community Atmosphere Model, J. Climate, 22, 3449–3469, doi:10.1175/2008JCLI2557.1, 2009.
Phillips, V. T. J., DeMott, P. J., and Andronache, C.: An empirical parameterization of heterogeneous ice nucleation for multiple chemical species of aerosol, J. Atmos. Sci., 65, 2757–2783, doi:10.1175/2007JAS2546.1, 2008.
Pitter, R. L. and Pruppacher, H. R.: A wind tunnel investigation of freezing of small water drops falling at terminal velocity in air, Q. J. Roy. Meteor. Soc., 99, 540–550, doi:10.1002/qj.49709942111, 1973.
Prenni, A. J., DeMott, P. J., Kreidenweis, S. M., Harrington, J. Y., Avramov, A., Verlinde, J., Tjernström, M., Long, C. N., and Olsson, P. Q.: Can ice-nucleating aerosols affect arctic seasonal climate?, B. Am. Meteorol. Soc., 88, 541–550, doi:10.1175/BAMS-88-4-541, 2007.
Pruppacher, H. R., Klett, J. D., and Wang, P. K.: Microphysics of Clouds and Precipitation, Atmospheric and Oceanographic Sciences Library, Kluwer Academic Publishers, Dordrecht, the Netherlands, 1997.
Richardson, M. S., DeMott, P. J., Kreidenweis, S. M., Cziczo, D. J., Dunlea, E. J., Jimenez, J. L., Thomson, D. S., Ashbaugh, L. L., Borys, R. D., Westphal, D. L., Casuccio, G. S., and Lersch, T. L.: Measurements of heterogeneous ice nuclei in the western United States in springtime and their relation to aerosol characteristics, J. Geophys. Res.-Atmos., 112, D02209, doi:10.1029/2006JD007500, 2007.
Rogers, D. C., DeMott, P. J., Kreidenweis, S. M., and Chen, Y.: A continuous-flow diffusion chamber for airborne measurements of ice nuclei, J. Atmos. Ocean. Tech., 18, 725–741, doi:10.1175/1520-0426(2001)018<0725:ACFDCF>2.0.CO;2, 2001.
Rosinski, J., Haagenson, P. L., Nagamoto, C. T., and Parungo, F.: Nature of ice-forming nuclei in marine air masses, J. Aerosol Sci., 18, 291–309, doi:10.1016/0021-8502(87)90024-3, 1987.
Rosinski, J., Nagamoto, C. T., and Zhou, M. Y.: Ice-forming nuclei over the East China Sea, Atmos. Res., 36, 95–105, doi:10.1016/0169-8095(94)00029-D, 1995.
Seland, Ø., Iversen, T., Kirkevåg, A., and Storelvmo, T.: Aerosol-climate nteractions in the CAM-Oslo atmospheric GCM and investigation of associated basic shortcomings, Tellus A, 60, 459–491, doi:10.1111/j.1600-0870.2008.00318.x, 2008.
Sullivan, R. C., Petters, M. D., DeMott, P. J., Kreidenweis, S. M., Wex, H., Niedermeier, D., Hartmann, S., Clauss, T., Stratmann, F., Reitz, P., Schneider, J., and Sierau, B.: Irreversible loss

ACPD
14, 7141–7186, 2014

of ice nucleation active sites in mineral dust particles caused by sulphuric acid condensation, Atmos. Chem. Phys., 10, 11471–11487, doi:10.5194/acp-10-11471-2010, 2010.
Vali, G.: Nucleation terminology, J. Aerosol Sci., 16, 575–576, 1985.
Wang, M., Ghan, S., Ovchinnikov, M., Liu, X., Easter, R., Kassianov, E., Qian, Y., and Morrison, H.: Aerosol indirect effects in a multi-scale aerosol-climate model PNNL-MMF, Atmos. Chem. Phys., 11, 5431–5455, doi:10.5194/acp-11-5431-2011, 2011.
Welti, A., Lüönd, F., Kanji, Z. A., Stetzer, O., and Lohmann, U.: Time dependence of immersion freezing: an experimental study on size selected kaolinite particles, Atmos. Chem. Phys., 12, 9893–9907, doi:10.5194/acp-12-9893-2012, 2012.
Wheeler, M. J. and Bertram, A. K.: Deposition nucleation on mineral dust particles: a case against classical nucleation theory with the assumption of a single contact angle, Atmos. Chem. Phys., 12, 1189–1201, doi:10.5194/acp-12-1189-2012, 2012.
Wiacek, A. and Peter, T.: On the availability of uncoated mineral dust ice nuclei in cold cloud regions, Geophys. Res. Lett., 36, L17801, doi:10.1029/2009GL039429, 2009.
Xie, S., Boyle, J., Klein, S. A., Liu, X., and Ghan, S.: Simulations of Arctic mixed-phase clouds in forecasts with CAM3 and AM2 for M-PACE, J. Geophys. Res.-Atmos., 113, D04211, doi:10.1029/2007JD009225, 2008.
Xie, S., Liu, X., Zhao, C., and Zhang, Y.: Sensitivity of CAM5-simulated Arctic clouds and radiation to ice nucleation parameterization, J. Climate, 26, 5981–5999, doi:10.1175/JCLI-D-12-00517.1, 2013.
Young, K. C.: The role of contact nucleation in ice phase initiation in clouds, J. Atmos. Sci., 31, 768–776, doi:10.1175/1520-0469(1974)031<0768:TROCNI>2.0.CO;2, 1974.
Zender, C. S., Bian, H., and Newman, D.: Mineral Dust Entrainment and Deposition (DEAD) model: description and 1990s dust climatology, J. Geophys. Res.-Atmos., 108, 4416, doi:10.1029/2002JD002775, 2003.
Zhang, G. J. and McFarlane, N. A.: Sensitivity of climate simulations to the parameterization of cumulus convection in the Canadian Climate Centre general circulation model, Atmos. Ocean, 33, 407–446, 1995.
Zimmermann, F., Weinbruch, S., Schütz, L., Hofmann, H., Ebert, M., Kandler, K., and Worringen, A.: Ice nucleation properties of the most abundant mineral dust phases, J. Geophys. Res.-Atmos., 113, 8576, doi:10.1029/2008JD010655, 2008.

ACPD
14, 7141–7186, 2014

Zobrist, B., Koop, T., Luo, B. P., Marcolli, C., and Peter, T.: Heterogeneous ice nucleation rate coefficient of water droplets coated by a nonadecanol monolayer, J. Phys. Chem. C, 111, 2149–2155, doi:10.1021/jp066080w, 2007.

ACPD
14, 7141–7186, 2014

Table 1. Parameters for the ice nucleation parameterization in single contact angle (α) model. In the table, DeMott et al. (2011) and Koehler et al. (2010) are Saharan Dust. $\Delta g^{\#}$ is the activation energy; $f_{i,max,x}$ is the maximum ice nucleating fraction.

Aerosol	Reference	Nucleation mode	α (°)	$\Delta g^{\#}$ (10^{-20} J)	$f_{i,max,x}$
Soot	DeMott (1990)	Immersion	48.0	14.15	0.01
Dust	DeMott et al. (2011)	Immersion	46.0	14.75	1
Soot	Möhler et al. (2005)	Deposition	28.0	−20	0.01
Dust	Koehler et al. (2010)	Deposition	20.0	−0.81	1

ACPD
14, 7141–7186, 2014

Table 2. Fit parameters obtained for the two models for the immersion freezing by dust. The root mean square errors (RMSE) between the fit curves and the data are given. In the table, μ is the mean contact angle; σ is the standard deviation.

Model	Parameter/RMSE	CSU106	CSU108	ZINC106	ZINC108	ZINC110
Single-α	α (°)	46.0	47.0	61.0	61.0	59.0
	$\Delta g^{\#}$ (10^{-20} J)	14.75	14.4	13.5	13.45	13.65
	RMSE	0.029	0.236	0.087	0.0983	0.147
α-PDF	μ (°)	46.0	47.0	62.0	61.0	59.0
	σ	0.01	0.01	0.04	0.01	0.02
	RMSE	0.01	0.225	0.08	0.07	0.08

ACPD
14, 7141–7186, 2014

Table 3. Simulation descriptions.

Simulation	Description
CTL	CAM5 with the default heterogeneous ice nucleation parameterization (Meyers et al., 1992)
CNT	As in CTL, but with the classical nucleation theory based on Hoose et al. (2010), using new fitting parameters in Table 1 (e.g., for immersion freezing on dust: $\alpha = 46^{\circ}$, $\Delta g^{\#}(10^{-20}\,\mathrm{J}) = 14.75$)
PDF	As in CTL, but with the improved CNT by introducing α-PDF model in immersion freezing on dust ($\mu = 46^{\circ}$, $\sigma = 0.01$)
MU1	As in PDF, but with $\mu = 31^{\circ}$, $\sigma = 0.01$
MU2	As in PDF, but with $\mu = 61^{\circ}$, $\sigma = 0.01$
SD1	As in PDF but with $\mu = 46^{\circ}$, $\sigma = 0.04$ (4σ)
SD2	As in PDF but with $\mu = 46^{\circ}$, $\sigma = 0.08$ (8σ)

ACPD
14, 7141–7186, 2014

Table 4. Global annual mean fields for the present-day simulations and differences of these variables between present-day and preindustrial simulations. Variables listed in the table are: total cloud cover (TCC, %), low cloud cover (LCC, %), liquid water path (LWP, $g\,m^{-2}$), ice water path (IWP, $g\,m^{-2}$), shortwave cloud forcing (SWCF, $W\,m^{-2}$), longwave cloud forcing (LWCF, $W\,m^{-2}$) and integrated column ice number concentration in mixed-phase clouds (ICNUM, $10^3\,cm^{-2}$).

Run	CTL	CNT	PDF	MU1	MU2	SD1	SD2
TCC	64.	64.	63.9	64.	64.	64.	63.9
ΔTCC	0.14	0.47	0.36	0.42	0.45	0.57	0.39
LCC	43.6	43.1	43.	43.1	43.1	43.1	43.1
ΔLCC	0.32	0.69	0.62	0.68	0.59	0.76	0.65
LWP	44.59	46.82	46.02	46.06	46.49	46.52	46.47
ΔLWP	3.26	4.05	3.61	3.72	3.83	3.90	3.64
IWP	17.78	16.21	16.31	16.35	16.25	16.16	16.17
ΔIWP	0.14	0.33	0.40	0.39	0.42	0.37	0.29
SWCF	−52.00	−52.27	−51.99	−52.08	−52.23	−52.23	−52.20
ΔSWCF	−1.64	−2.02	−1.86	−1.96	−2.02	−2.07	−1.88
LWCF	24.04	23.65	23.61	23.64	23.66	23.66	23.63
ΔLWCF	0.50	0.82	0.81	0.84	0.83	0.88	0.75
CF	−27.96	−28.62	−28.38	−28.45	−28.58	−28.57	−28.57
ΔCF	−1.14	−1.20	−1.05	−1.12	−1.19	−1.19	−1.13
ICNUM	2.863	2.388	2.417	2.419	2.394	2.364	2.387
ΔICNUM	0.036	0.076	0.086	0.063	0.071	0.052	0.054

ACPD
14, 7141–7186, 2014

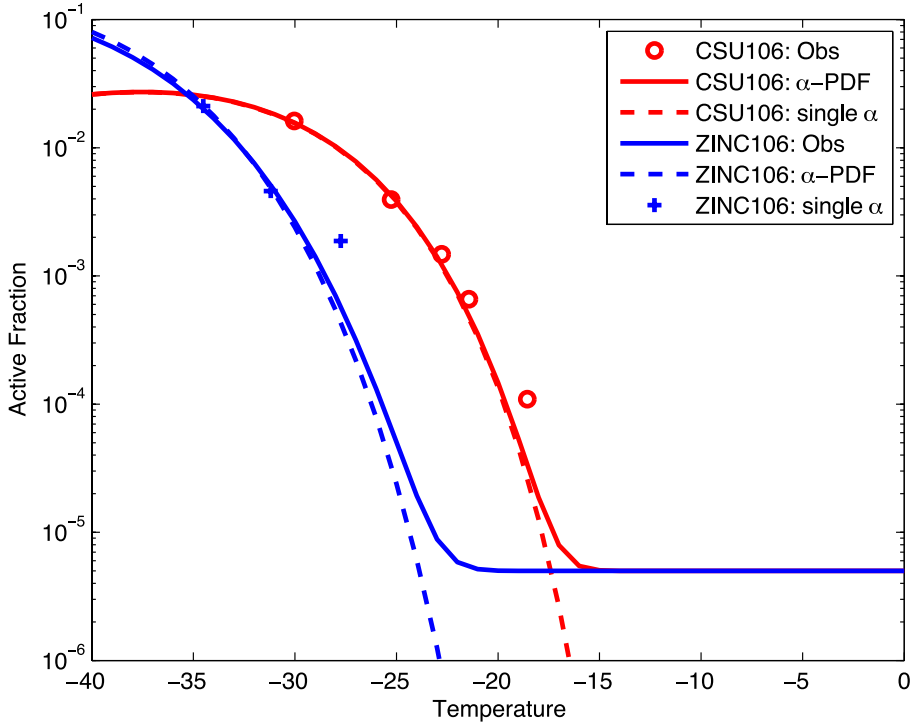

Fig. 1. Active fractions determined with CSU106 and ZINC106 respectively (DeMott et al., 2011) are presented as a function of temperature T (indicated by the different symbols). The different lines represent the single-α model and the α-PDF model results fitting the experimentally determined active fractions (parameters in two models are given in the Table 2).

ACPD
14, 7141–7186, 2014

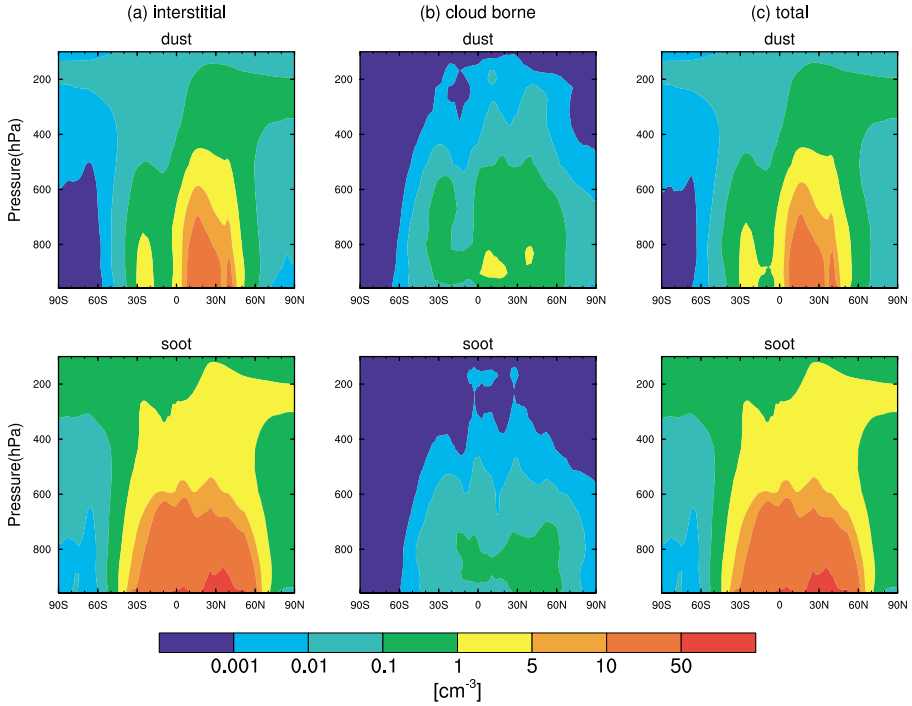

Fig. 2. Zonal annual mean number concentrations (cm^{-3}) of **(a)** interstitial, **(b)** cloud borne and **(c)** total mineral dust (upper) and soot particles (lower).

ACPD
14, 7141–7186, 2014

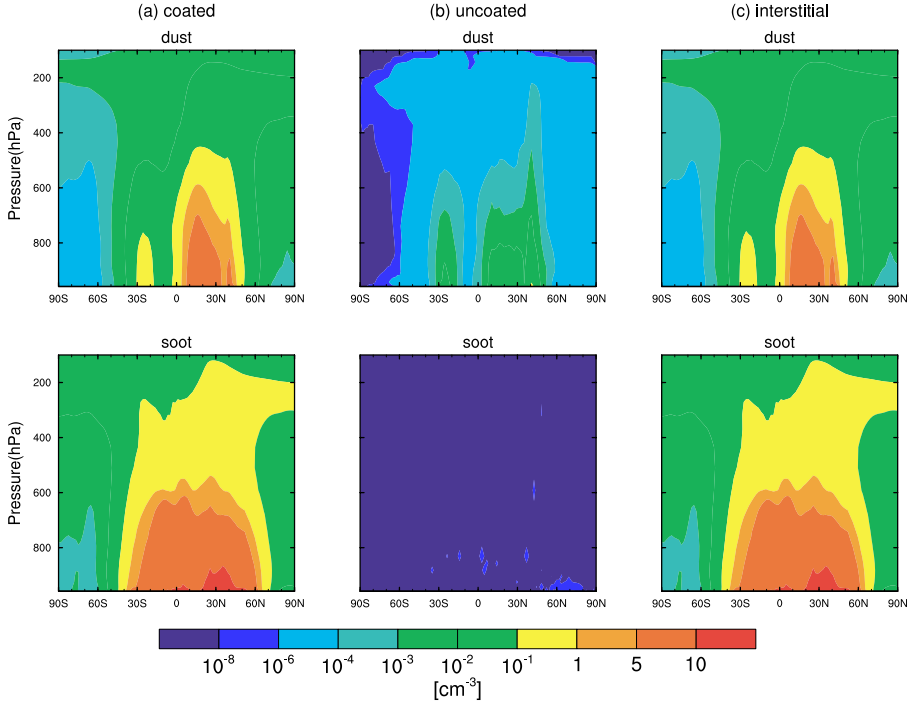

Fig. 3. Zonal annual mean number concentrations of **(a)** interstitial coated, **(b)** interstitial uncoated and **(c)** total interstitial mineral dust (upper) and soot particles (lower).

ACPD
14, 7141–7186, 2014

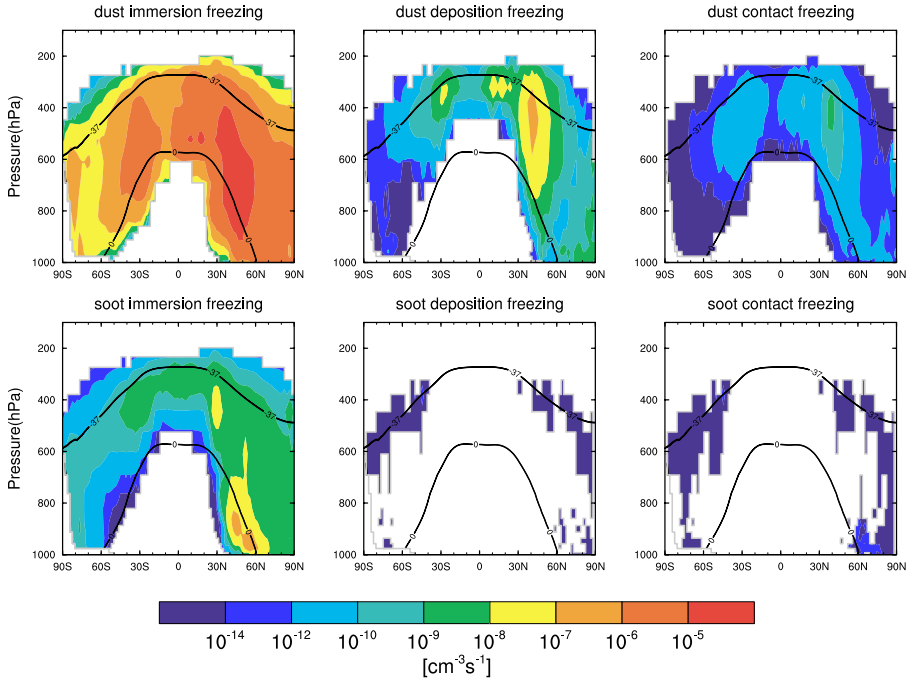

Fig. 4. Zonal and annual mean immersion, deposition, and contact freezing rates in the PDF simulation. Isotherms of 0 °C and −37 °C are plotted.

ACPD
14, 7141–7186, 2014

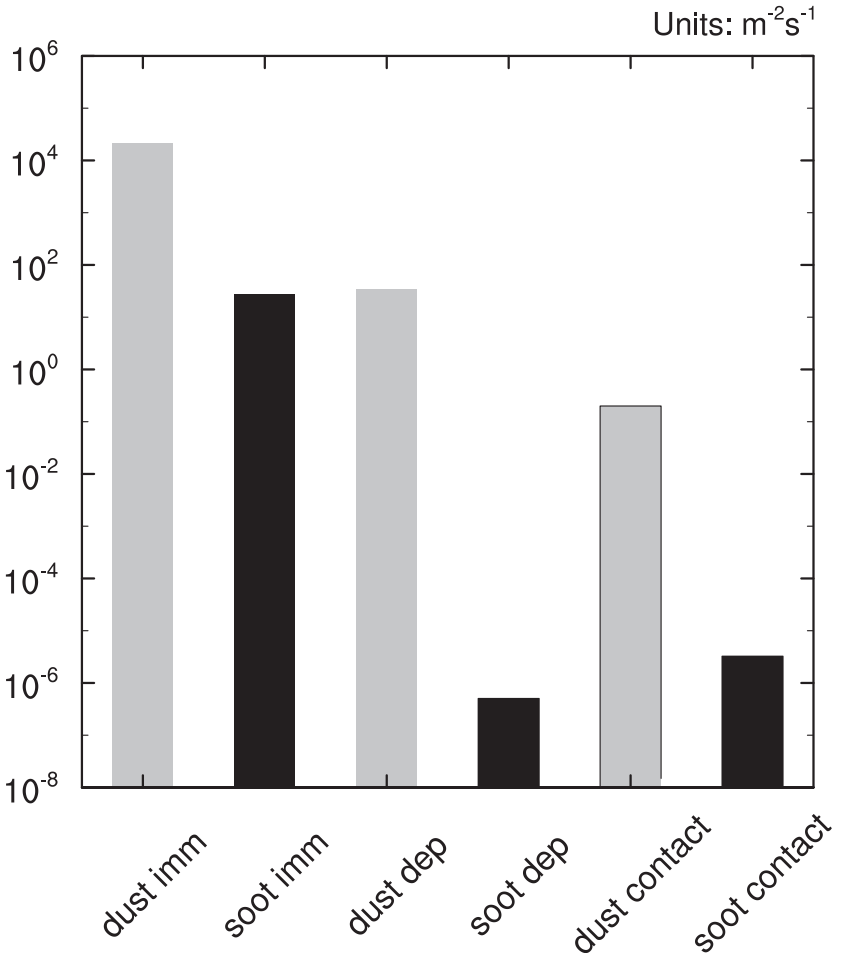

Fig. 5. Global and annual mean vertically integrated nucleation rates in the PDF simulation.

ACPD
14, 7141–7186, 2014

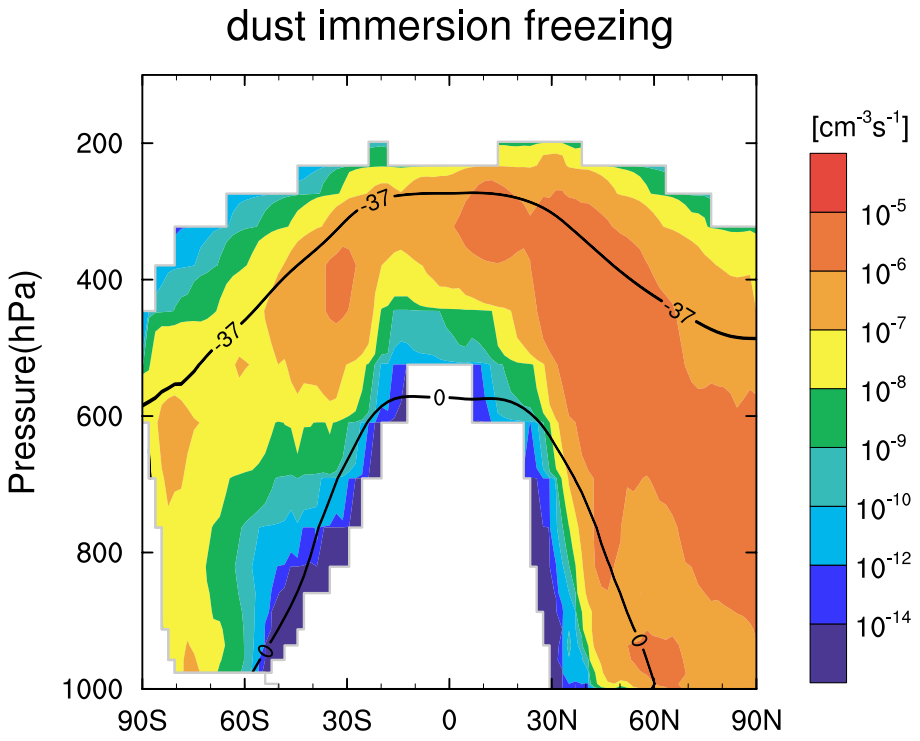

Fig. 6. Zonal annual mean immersion freezing rates in the CNT simulation. Isotherms of 0 °C and −37 °C are plotted.

ACPD
14, 7141–7186, 2014

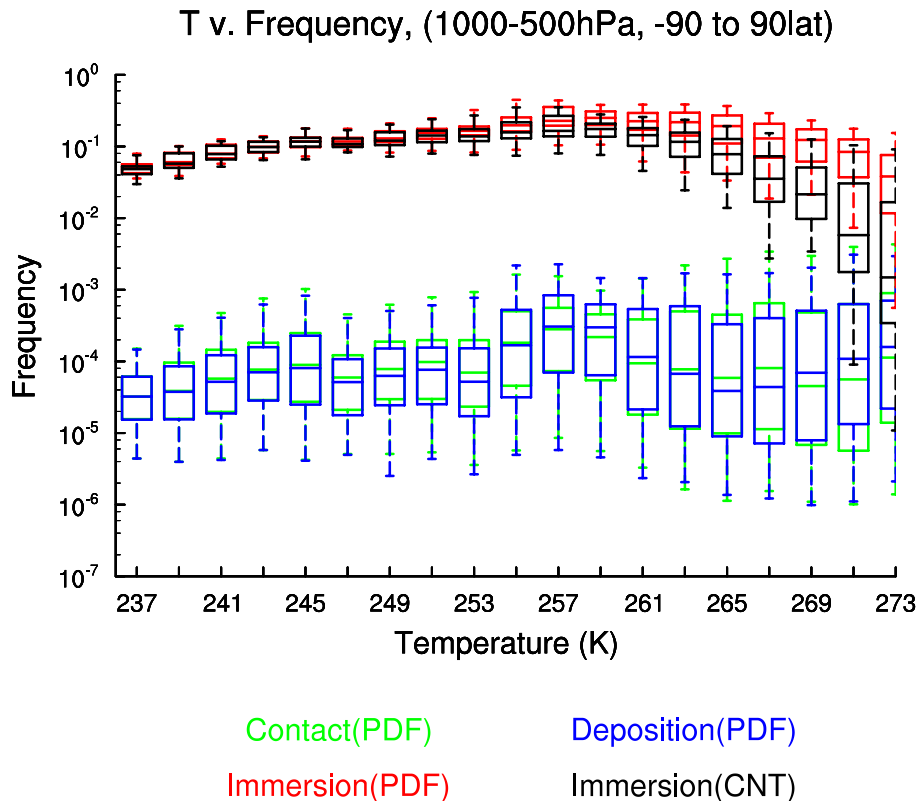

Fig. 7. Annual mean simulated frequency of immersion freezing (red), deposition nucleation (blue) and contact nucleation (green) in the PDF simulation, and immersion freezing (black) in the CNT simulation as a function of temperature. The whiskers represent the 5th and 95th percentiles, and the boxes represent the 25th and 75th percentiles and the median.

ACPD
14, 7141–7186, 2014

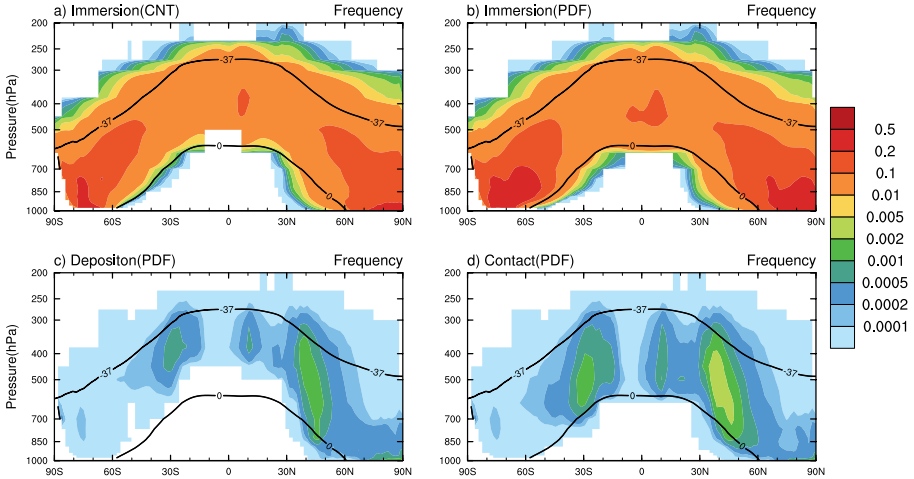

Fig. 8. Zonal and annual mean distribution of occurrence frequency of **(a)** immersion mode in the CNT simulation, and of **(b)** immersion, **(c)** deposition, and **(d)** contact freezing modes in the PDF simulation. Isotherms of 0 °C and −37 °C are plotted.

ACPD
14, 7141–7186, 2014

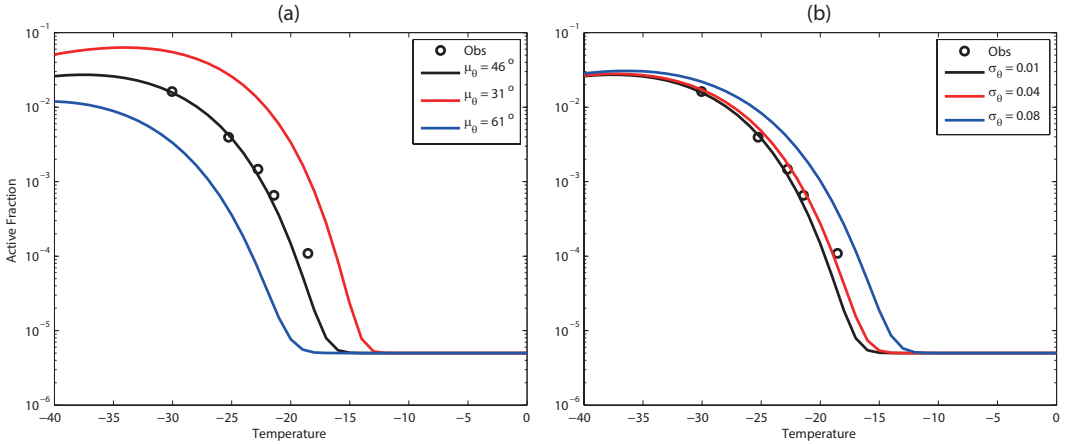

Fig. 9. Active fraction as a function of temperature for given the α-PDF model settings. Observation data is from CSU106 and the black solid line is its fit curve. The red and blue solid lines are sensitivity tests to **(a)** mean contact angle, and **(b)** standard deviation.

ACPD
14, 7141–7186, 2014

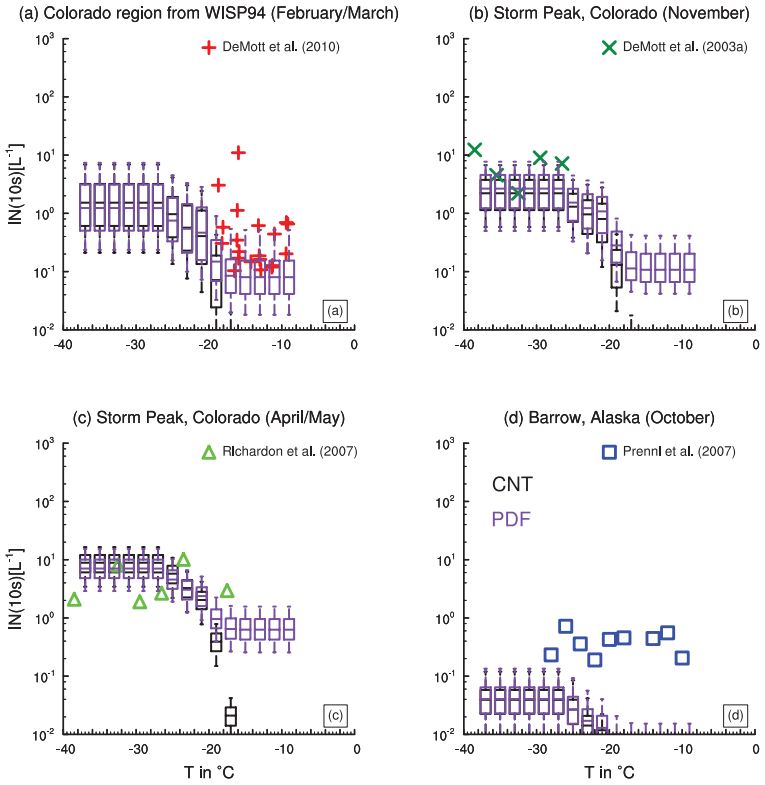

Fig. 10. IN(10 s) concentrations for specified temperature, selected at the grid points including the measurement locations and at the same pressure level as field observations in the CNT simulation (black boxes and whiskers) and in the PDF simulation (blueviolet boxes and whiskers). The whiskers represent the 5th and 95th percentiles, and the boxes represent the 25th and 75th percentiles and the median. The colored symbols indicate CFDC IN measurements.

ACPD
14, 7141–7186, 2014

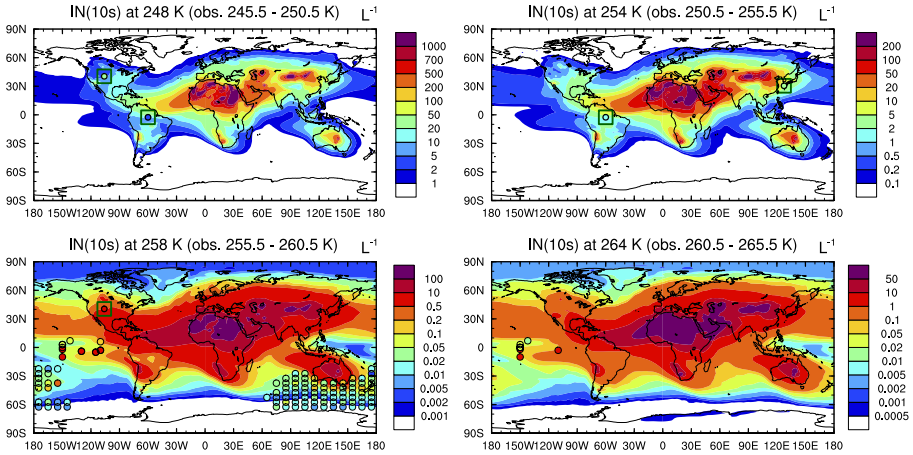

Fig. 11. Spatial comparison of IN(10 s) concentration with field data. IN(10 s) concentrations are sampled for four specific temperatures which fall into the same range of observed temperatures as chosen for measurements on the surface. The field IN measurements are indicated by colored circles (DeMott et al., 2010, in Central USA; Rosinski et al., 1987, in Central Pacific; Rosinski et al., 1995, in East China Sea; Bigg et al., 1973, in South of Australia). Especially, field IN measurements at East China Sea, Brazil and Central USA are highlighted by darkgreen rectangles to see clearly.

ACPD
14, 7141–7186, 2014

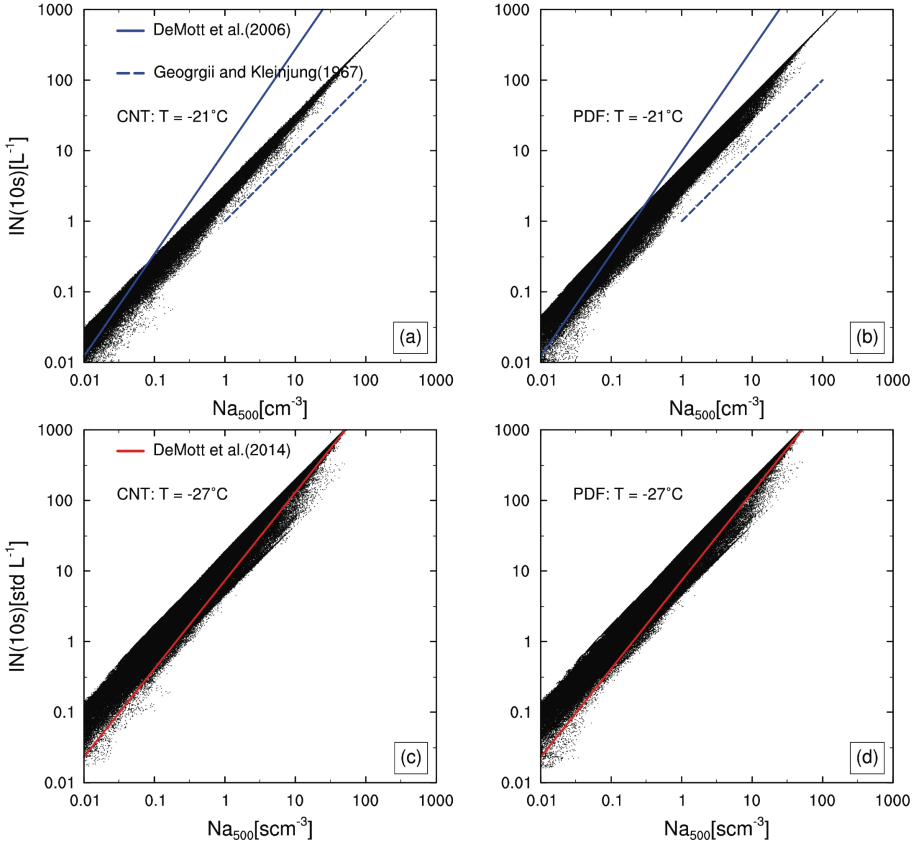

Fig. 12. IN(10 s) concentrations in the CNT and PDF simulations, displayed as a function of the number concentrations of aerosol particles with $d > 0.5\,\mu m$ at (**a** and **b**) $T = -21\,^{\circ}C$ which is the observed temperature used in the power-law fit to observations (DeMott et al., 2006, (blue solid line); Georgii and Kleinjung, 1967 (blue dash line)) and at (**c** and **d**) $T = -27\,^{\circ}C$ which is used for the DeMott et al. (2014) proposed parameterization (solid red line).

ACPD
14, 7141–7186, 2014